REVIEW

Continuous-Flow Syntheses of Alloy Nanoparticles

Kohei Kusada[*a, b] and Hiroshi Kitagawa [*c]

Alloy nanoparticles (NPs), including core-shell, segregated and solid-solution types, show a variety of attractive properties such as catalytic and optical properties and are used in a wide range of applications. Precise control and good reproducibility in the syntheses of alloy NPs are highly demanded because these properties are tunable by controlling alloy structures, compositions, particle sizes, and so on. To improve the efficiency and reproducibility of their syntheses, continuous-flow syntheses with various types of reactors have recently been developed instead of the current mainstream approach, batch syntheses. In this review, we focus on the continuous-flow syntheses of alloy NPs and first overview the flow syntheses of NPs, especially of alloy NPs. Subsequently, the details of flow reactors and their chemistry to synthesize core-shell, segregated, solid-solution types of alloy NPs, and high-entropy alloy NPs are introduced. Finally, the challenges and future perspectives in this field are discussed.

1. Introduction

Nanoparticles (NPs) having an extremely large surface-to-volume ratio are widely studied and used for a variety of applications because of their unique properties such as catalytic and optical properties. These properties are tunable by controlling the particle size and shape, and therefore, many kinds of syntheses for nanosized metals, ceramics, semiconductors, and metal complexes such as metal-organic frameworks have been investigated.[1–3]

Alloy is one of the hot topics in nanomaterials science because alloy NPs often show unique physical and chemical properties that cannot be observed in or are superior to monometallic NPs.[4,5] To improve their properties, various types of alloy NPs have been developed. For example, core shell-type alloy NPs, which are unique nanostructured alloys, are heterostructures that have an inner core metal structure and an outer thin shell of a different metal. The electronic and geometric structures of thin outer metal are largely influenced by an inner core metal, resulting in the emergence of new properties of the outer shell metal.[6] As another example, solid-solution alloy NPs are homogeneous structures where several constituents are randomly and homogeneously mixed at the atomic level. Therefore, the constituent atoms interact with each other, leading to attractive properties of solid-solution alloys because the unique local and total electronic structures are very different from the mother metals.[7,8] Although the synthesis techniques to precisely control these alloy structures such as core-shell structure and shape-controlled NPs have been well developed, many of the syntheses are basically based on batch-type techniques that are not suitable for mass production because of their small yields and nonuniform reaction conditions. Therefore, more effective methods for mass

a. The Hakubi Centre for Advanced Research, Kyoto University, Kitashirakawa-Oiwakecho, Sakyo-ku, Kyoto 606-8502. E-mail: kusada@kuchem.kyoto-u.ac.jp
b. PRESTO, Japan Science and Technology Agency, 4-1-8 Honcho, Kawaguchi, Saitama 332-0012.
c. Division of Chemistry, Graduate School of Science, Kyoto University, Kitashirakawa-Oiwakecho, Sakyo-ku, Kyoto 606-8502, Japan. E-mail: kitagawa@kuchem.kyoto-u.ac.jp

Kohei Kusada

Kohei Kusada received his Ph.D. in 2013 at Kyoto University under the supervision of Prof. Hiroshi Kitagawa. He worked as a researcher at Asahi Kasei Chemicals Co. (2013–2014) and then moved back to Kyoto University as an Assistant Professor in Prof. Kitagawa's laboratory. He became an Associate Professor of the Hakubi centre at Kyoto University in 2021. He has also been a researcher for the Japan Science and Technology Agency (JST), Precursory Research for Embryonic Science and Technology (PRESTO). His current research interests focus on the design of advanced functional nanoparticles for catalysis.


Hiroshi Kitagawa

Hiroshi Kitagawa was born in December 1961 in Osaka, finished his Ph.D. at Kyoto University in 1991 and, after working as an Assistant Professor at the Institute for Molecular Science (IMS) and Japan Advanced Institute of Science and Technology (JAIST), he was appointed as an Associate Professor at the University of Tsukuba in 2000. He became a Professor of Chemistry at Kyushu University in 2003 and moved to Kyoto University as a Professor in 2009. He was Vice Provost and Deputy Executive-Vice President for Research at Kyoto University. He was also engaged at JST as a Research Director of ACCEL and is a Director of the network-type research institution Science and Creation of Innovative Catalysts, PRESTO. He has published more than 430 original research papers dealing with solid-state chemistry, coordination chemistry, nanoscience, low-dimensional electron systems, and molecular-based conductors.

production are required for the practical application of alloy NPs in the industry.

A continuous-flow system is suitable for mass production because a flow-reaction system gives highly efficient productivity with high reproducibility because of stable reaction conditions. Also, from a viewpoint of green sustainable chemistry, flow syntheses are more energy-efficient and more favourable than a batch process.[9–11] For example, a flow synthesis is performed in a small reactor requiring a smaller heater/chiller and discharge little wastes, compared to a batch synthesis. Therefore, flow chemistry has been well studied to synthesize organic molecules from simple small organic molecules to complicated pharmaceutical molecules.[12] Furthermore, continuous-flow methods have also been applied to synthesize inorganic nanomaterials such as metals, semiconductors, and oxides.[13,14] Although several reports summarize the continuous-flow syntheses of inorganic nanomaterials with the object of supercritical fluid, microfluid reactors, and so on,[15–17] the syntheses of alloy NPs in flow chemistry have not been reviewed yet. In this review, we focus on the continuous-flow syntheses of alloy NPs. First, the flow syntheses of NPs are overviewed. Subsequently, the details of flow reactors and their chemistry to synthesize core-shell, segregated, solid-solution types of alloy NPs, and high-entropy alloy (HEA) NPs that are newly developed alloy materials are introduced. Finally, the challenges and future perspectives in this field are discussed.

2. Flow Syntheses of Nanoparticles

2. 1. Overview of flow syntheses of nanoparticles
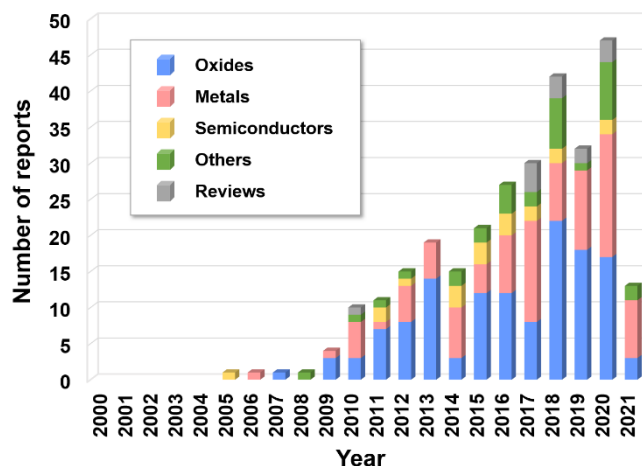
Fig. 1 The number of research articles including the keywords "flow-synthesis*" and "nanoparticles*" (searched through Web of Science in June 2021). Blue, oxides; red, metals; yellow, semiconductors; green, others; gray, reviews.

First, to overview the studies on continuous-flow syntheses for nanomaterials, we surveyed the number of research papers including the keywords "flow-synthesis*" and "nanoparticles*" through the Web of Science. In Figure 1, blue, red, yellow, and green colours show the number of reports about the flow syntheses of oxide NPs, metallic NPs, semiconductor NPs, and others, respectively. Gray indicates comprehensive reviews, including various kinds of NPs. Although only a few studies were

Table 1 Alloy NPs synthesized in flow reactors and their synthesis conditions

Element	Structure	Size	Temp.	Pressure	Reductant	Solvent	Protecting agent	Support	Step (technique)	Properties	Ref.
AuAg, AuAgAu	Core shell	~50 nm	RT	1 bar	Ascorbic acid	H_2O	CTAB	N/A	Multi (micro segmentaion)	Optical	38
PtRu	Solid solution	N/A	450 °C	200 bar	EtOH	EtOH	N/A	N/A	Single (high pressure)	N/A	72
AgRh	Solid solution	N/A	120 °C	1 bar	EG[1]	EG	PVP	N/A	Single (microwave)	Catalysis	61
PtPb	Solid solution	45 nm	330 °C	250 bar	EtOH	EtOH	N/A	N/A	Single (high pressure)	N/A	31
PdNi	Segregated (Pd on Ni)	N/A	204 °C	1 bar	Benzyl Alcohol	Benzyl Alcohol	Oleylamine	Ni	Multi (microwave)	Catalysis	50
AuPd	Core shell	> 50nm	RT	1 bar	Ascorbic acid	Water in dodecane	PVP	N/A	Multi (electrocoalescence)	N/A	42
PdPt	Core shell	20-30 nm	96 °C	1 bar	Ascorbic acid	H_2O	CTAB	N/A	Single	Catalysis	54
PdPt, PdPtFe	Solid solution	2-3 nm	300 °C	280 bar	EtOH	EtOH	N/A	γ-Al_2O_3	Single (high pressure)	Catalysis	73
AuPd	Core shell / solid solution	< 10 nm	RT	1 bar	$NaBH_4$	H_2O	PVA	TiO_2	Multi/ Single (in one flow)	Catalysis	40
AuPd	Solid solution	3-4 nm	RT	1 bar	$NaBH_4$	H_2O	PVA	TiO_2	Single	Catalysis	32
PtFeCu	Solid solution	1.8 nm	RT	1 bar	$H_3N \cdot BH_3$	H_2O, EG, PEG[2]	N/A	Carbon	Single (microchip)	Catalysis	64
PdPt	Core shell	4 nm	RT	1 bar	$NaBH_4$	H_2O	PVP	Carbon	Multi (in one flow)	N/A	41
PdPt PdRu, PdRuIr, PdRuIrPtRh(HEA)	Solid solution	~ 5nm	230 ~ 250 °C	~100 bar	EtOH	EtOH + H_2O	PVP	N/A	Single (high pressure)	Catalysis	76

[1] EG: ethylene glycol, [2] TEG: polyethylene glycol

reported in the 2000s,[18–22] the number of reports significantly increased and reached around 50 per year in 2020. In total, oxide, metallic, and semiconductor NPs have widely been studied and have occupied about 45%, 32% and 7% of the reports, respectively. In the oxide NPs, flow syntheses using supercritical water are well studied[23] because supercritical water (> 374 °C and > 22.1 MPa) has unique features such as a very low dielectric constant leading to the formation of metal oxides. In particular, the syntheses of FeO_x, TiO_x, ZnO_x, and CeO_x for applications including catalysis, magnetics, and ion conductors have been investigated.[24–26] The flow syntheses of metallic NPs, including monometallic and alloy NPs, are also well studied. The syntheses of monometallic Au and Ag are the most well-studied topics[27–30] and account for approximately half of the reports. However, there are fewer reports about alloy NPs than monometallic NPs.[31,32] The details are explained in the next section. Other than those, the syntheses of semiconductors such as CdSe NPs and hydroxyapatite NPs were reported.[33,34] In addition, recently, metal-organic frameworks, including MIL-100, ZIF-8 and CPO-27, have also been synthesized by flow reactors.[35–37] Based on those reports, it could be concluded that flow syntheses can be applied to a lot of fast reactions, including oxidation, reduction, and complex formation reactions, which have attracted increasing attention in recent years.

2. 2. Flow syntheses of alloy nanoparticles

The syntheses of alloy NPs by flow reactors are summarized in Table 1. These studies have been reported since the 2010s, and most of them were reported in the past five years. Depending on the desired alloy structures, a suitable flow system is chosen. For example, multi-step type reactors were designed to
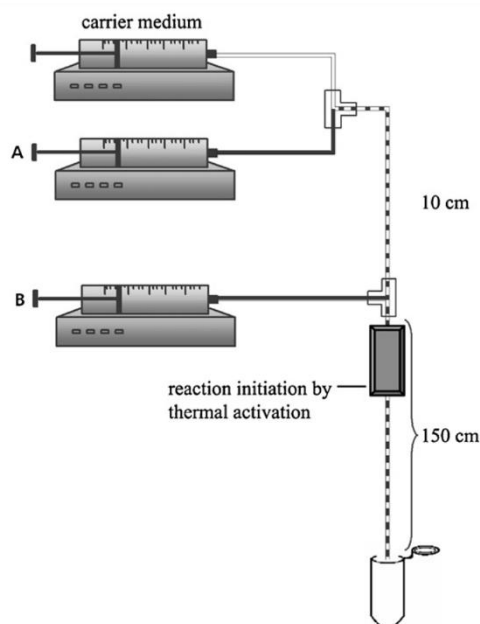
Fig. 2 Schematic of the micro-segmented flow reactor for Au@Ag and Au@Ag@Au core-shell alloy NPs. The solutions in syringes A and B are explained in the main text. Reproduced with permission from ref. 38 Copyright 2011, Elsevier.

sequentially reduce different metal ions and form core-shell type structures, while single-step reactors inducing concurrent reduction of metal ions seem to be suitable for synthesizing solid-solution alloy NPs. Furthermore, in the case of core-shell type structure, additives such as ascorbic acid and $NaBH_4$ are used as reducing agents and supercritical EtOH is often used as a reducing agent for solid-solution alloy NPs. As with the monometallic NPs' case, Au- and/or Ag-based alloy NPs are studied, and platinum group metals such as Pt- and Pd-based alloy NPs have also been studied. In addition, for catalytic applications, some alloy NPs were synthesized directly on oxide or carbon supports without protecting agents. The details, including flow systems, reactors, and synthesis conditions, are discussed in the following sections.

3. Flow Syntheses of Core-Shell Type or Segregated Type Nanoparticles

Because the core-shell structure has an inner core metal and an outer thin shell of a different metal, sequential reduction of metal ions is required for the bottom-up synthesis. In this section, flow-reaction systems and strategies for core-shell alloy NPs are introduced.
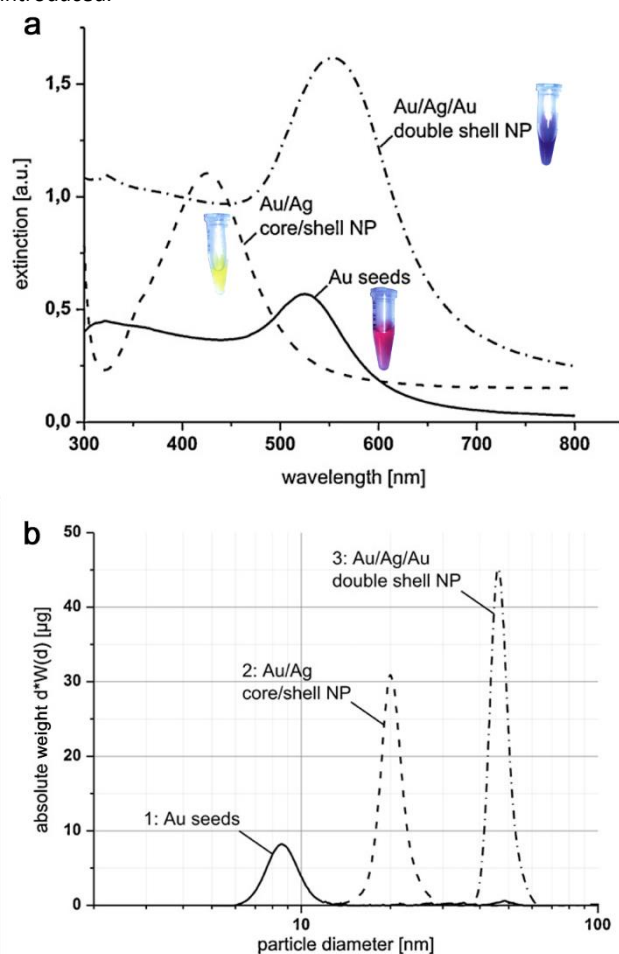
Fig. 3 a) Absorption spectra and optical images, and b) DCS spectra of the Au, Au@Ag and Au@Ag@Au NPs. Reproduced with permission from ref. 38 Copyright 2011, Elsevier.

3. 1. Continuous micro-segmented flow synthesis

The first example was reported in 2011 by A. Knauer et al.[38] They synthesized Au@Ag and Au@Ag@Au core-shell alloy NPs by a micro-segmented technique (Fig. 2). This technique uses small droplets (segments) of the reactant mixture generated by injection into an immiscible liquid carrier that inhibits fusion between reagents and the reactor tubes.[39] Also, this technique induces rapid mixing and reduced dispersion, resulting in the synthesis of monodispersed NPs.[16,18,39] In Fig. 2, the segmented flow is generated by two immiscible liquid flows, the carrier media (tetradecane) and the reactant solution, united in a PTFE T-junction. For the synthesis of Au@Ag, a mixture of aqueous solutions of Au seeds, AgNO₃, ascorbic acid (reductant) and cetyltrimethylammonium bromide (CTAB, protecting agent) was loaded in syringe A. NaOH aqueous solution was injected into the segmented flow by syringe B, and the solution was heated at 80 °C. In the case of Au@Ag@Au double-shell NPs, a mixture of Au@Ag seeds and ascorbic acid and HAuCl₄ aqueous solution were injected by syringes A and B, respectively without heating. Fig. 3a shows the absorption spectra and optical images of the Au, Au@Ag and Au@Ag@Au NPs prepared by the segmented flow synthesis. The absorption spectra were blue-shifted and had a narrower bandwidth than the alloy NPs prepared by batch synthesis, indicating that the flow synthesis provided homogeneous particle sizes and shapes. This is confirmed by differential centrifugal sedimentation (DCS) (Fig. 3b). The narrower size distribution and smaller particle size are caused by the effective mixing of the reactants in the micro segments due to the fast segment internal conversion.
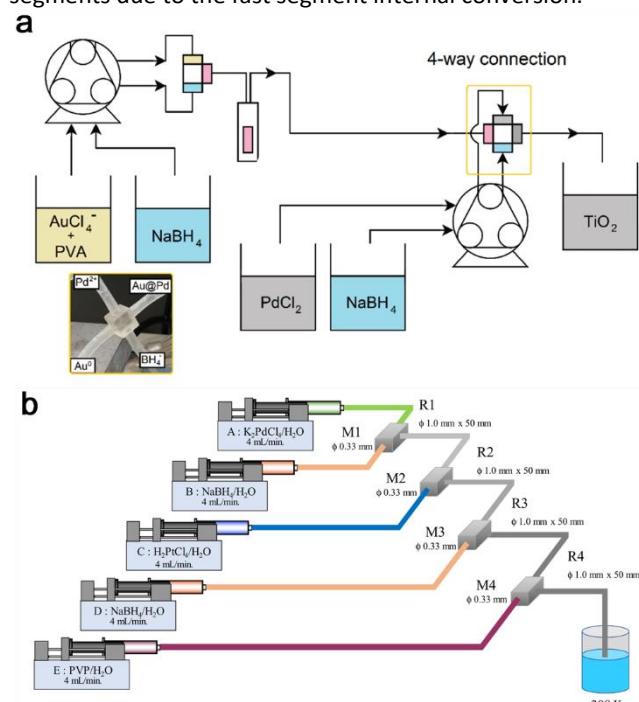
Fig. 4 Schematics of multi-step flow reactors for a) Au@Pd (the inset is the 3D printed 4-way connection) and b) Pd@Pt core-shell NPs. Reproduced with permission from ref. 40 Copyright 2019, Royal Society of Chemistry; ref. 41 Copyright 2021, Elsevier.
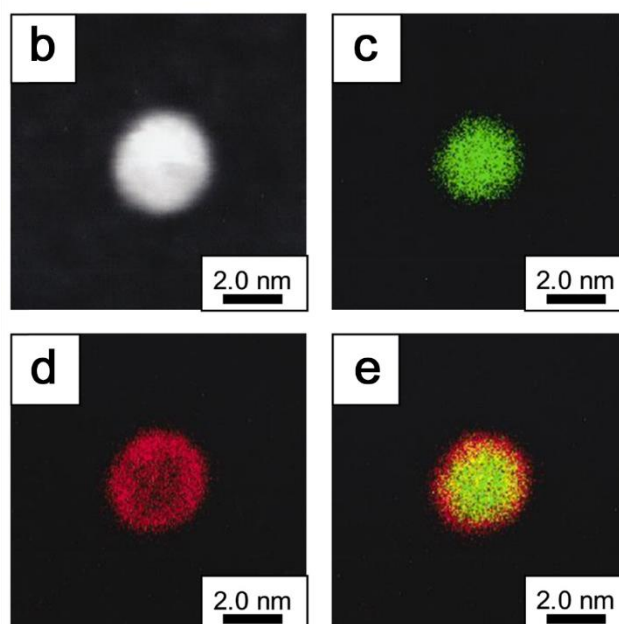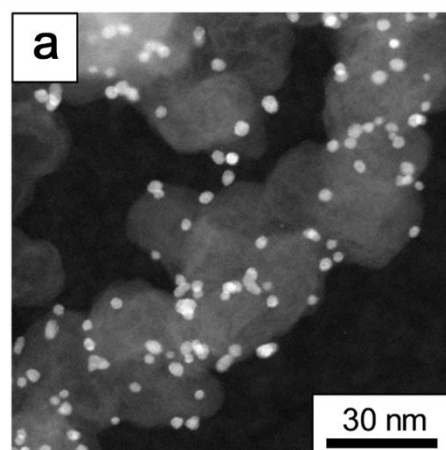
Fig. 5 (a) DF-STEM image of Pd@Pt. (b) DF-STEM image and its EDS maps of (c) Pd and (d) Pt and (e) Pd + Pt. Reproduced with permission from ref. 41 Copyright 2021, Elsevier.

3. 2. Multi-step reactions in one flow synthesis

The production of Au@Pd through multi-step reactions in one flow system was done by Cattaneo et al.[40] In Fig. 4a, a mixture of Au precursor (HAuCl₄) and protecting agent (polyvinyl alcohol; PVA) aqueous solutions was mixed with a reducing agent (NaBH₄) solution in a T-shape connector by using a two-channel peristaltic pump, resulting in the formation of Au NPs confirmed by *on-stream* UV-vis spectrometry (the red square after the T-shaped connector in Fig. 4a). Then, the thin Pd shell on the surface of pre-synthesized Au NPs was formed by the selective reduction of PdCl₂ through the mixing of the three solutions (Au NPs, Pd precursor and NaBH₄) in a 4-way connection. The colloidal solution was added into a TiO₂ solution, and the NPs were immobilized on TiO₂.

Similarly, Fujitani et al. synthesized Pd@Pt core-shell NPs.[41] As shown in Fig. 4b, they used syringe pumps to feed solutions and T-shaped connectors to mix the solutions. All solutions flowed at 4 ml/min and the diameters of the mixers and tubes were ø

0.33 mm and ø 1.0 mm. K_2PdCl_4 was first reduced by $NaBH_4$ at M1 and formed Pd NPs, and then H_2PtCl_4 and $NaBH_4$ were subsequently mixed into the solution at M2 and M3, respectively. After the formation of Pt shell on the surface of Pd NPs, a protecting agent (polyvinylpyrrolidone; PVP) aqueous solution was added as M4. The NPs can be directly supported on carbon without PVP by discharging the solution from the reactor after M3 into carbon slurry. The dark-field (DF) scanning transmission electron microscope (STEM) image and EDS maps showed that the synthesized NPs have a homogeneous particle size (3.6 nm) and clear core-shell structure (Fig. 5).

3. 3. Multi-step reactions assisted by electrocoalescence

Microfluidic droplets as introduced in Section 3.1 have been widely used as reaction vessels for many applications. Generally, once droplets are generated in a flow tube, it is difficult to inject new chemicals into the droplets for multi-step reactions. However, core-shell type alloy NPs are usually synthesized by subsequent reactions. Hatton et al. reported a method that uses a high-strength alternating electrical field (~10,000 V cm^{-1}) to selectively inject chemicals into the microdroplets with nanodroplets (mini-emulsion) (Fig. 6a).[42] The nanodroplets, which are typically in the 50-500-nm range and stably dispersed in an immiscible solvent by a surfactant, play a role of carriers for chemicals.[43,44] Nanodroplets were prepared by sonicating a mixture of dodecane and aqueous solution. Fig. 6b shows the three-step synthesis for Au@Pd core-shell NPs through electrocoalescence. In the first step, $HAuCl_4$ and PVP aqueous microdroplets were formed in the ascorbic acid miniemulsion. The microdroplets and miniemulsions were blended by passing through the electrical field, and Au NPs were formed. Then, Na_2PdCl_4 miniemulsion was injected into the flow and transferred into the microdroplets by the second
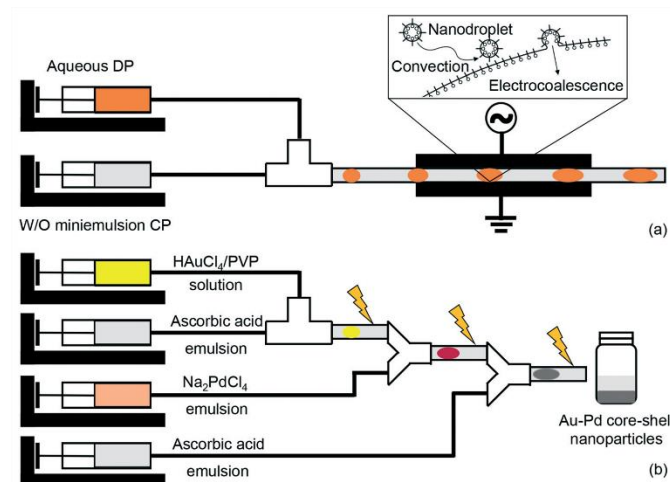
Fig. 6 (a) Schematics of the generation of aqueous microdroplets with a water/oil (W/O) miniemulsion by electrocoalescence. DP and CP represent the continuous phase and dispersed phase, respectively. (b) The setup for the synthesis of Au@Pd core-shell NPs through three electrocoalescence-assisted chemical addition steps. Reproduced with permission from ref. 42 Copyright 2018, Royal Society of Chemistry.
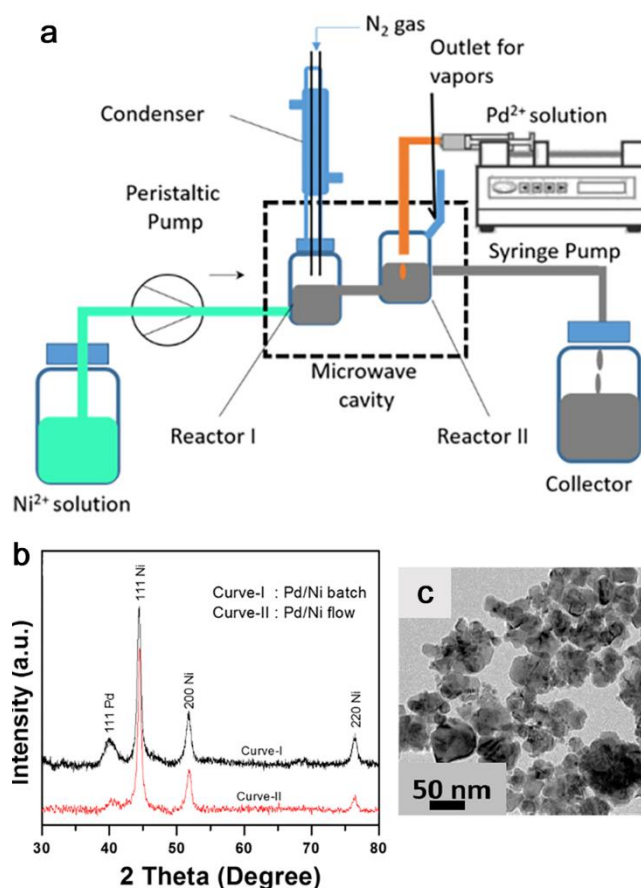
Fig. 7 (a) Schematic of microwave-assisted continuous-flow reactor for the sequential reduction of Ni and Pd ions. (b) Powder XRD patterns of Pd/Ni samples synthesized by batch (Curve-I) and flow (Curve-II) methods. (c) TEM image of Pd/Ni samples synthesized by the flow method. Reproduced with permission from ref. 50 Copyright 2017, American Chemical Society.

electrocoalescence. Afterward, the final electrocoalescence was done with ascorbic acid mini-emulsion and the Pd shell was formed on the surface of the pre-formed Au NPs. The prepared NPs showed the significant suppression of the Au surface plasmon resonance peak, but the residue peak indicated an insufficient coverage of Au NPs.[45] Also, TEM observation revealed that the Pd coating was not uniform, suggesting the secondary nucleation of Pd NPs occurred on Au NPs.

3. 4. Multi-step reactions assisted by microwave

Because using microwaves is an efficient heating method (72% less energy compared with a conventional heating process),[46] a combination of flow synthesis and microwave heating has been studied for high-throughput NPs synthesis.[47–49] Prasad et al. succeeded in synthesizing bimetallic NiPd NPs by a microwave-assisted continuous-flow reactor.[50] As shown in Fig. 7a, first Ni(II) acetate in benzyl alcohol with oleylamine was introduced to Reactor-I in the microwave cavity (700 W, 2.45 GHz) and maintained in the reactor for 5 min, resulting in the formation of Ni nanocrystals (NCs). Benzyl alcohol has good microwave

absorption capacity and works as a reducing agent under microwave irradiation.[51] After the overflow from Reactor-I, Ni NCs were introduced into Reactor-II where Pd(II) acetate in diphenyl ether was injected and remained there for 4 min under microwave irradiation. The product was extracted from the outlet. The product was characterized by XRD and TEM. The XRD pattern (Fig. 7b Curve-II) shows the peaks assigned to the 111 metallic Pd plane and 111, 200 and 220 metallic Ni planes. The Pd crystal size was estimated to be ~ 3 nm by Scherrer equation. The TEM image (Fig. 7c) confirms the small Pd NPs on larger Ni NCs. The synthesized NPs showed good catalytic activity for hydrogenation of aromatic nitro compounds and those bearing alkene and alkyne moieties.

3.5. Single-step flow synthesis

As mentioned, core shell-type NPs are often synthesized by multi-step reactions. However, some examples reported one-pot batch syntheses of core-shell NPs. For example, Pd@Pt core-shell NPs were obtained by a one-pot batch synthesis using ascorbic acid as a reducing agent.[52,53] Because the reduction rates of metal precursors should be different owing to the different redox potentials and reaction kinetics, it is possible to obtain core-shell NPs through one-pot synthesis by tuning the reduction rates of precursors.

Sebastian et al. reported one-step continuous-flow synthesis of Pd@Pt core-shell NPs with Pd nanocubes.[54] Fig. 8 shows a schematic of the reactor that has two inlet streams joined at a Y-shaped junction and a back regulator after the 4.2-m heated reactor coil. The first syringe was filled with a mixed aqueous solution of H_2PdCl_4, H_2PtCl_6 and CTAB (a protective agent). The second syringe was filled with an ascorbic acid solution as a
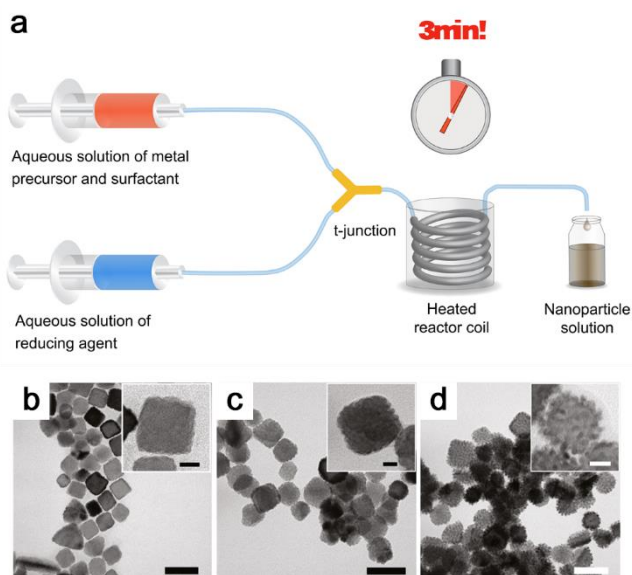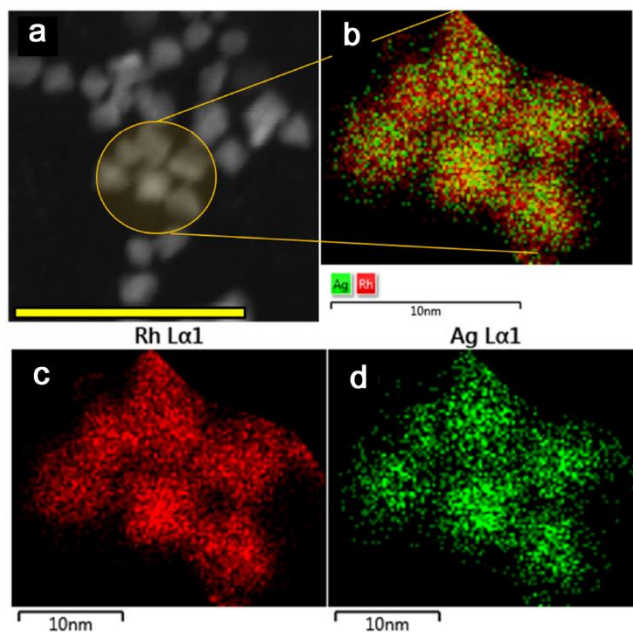
reducing agent. These syringes injected the solutions at the same rate, and the heater was set at 96 °C. Interestingly, in this synthesis, after only 3 min of heating, Pd@Pt NPs were formed, even though a batch synthesis requires 30 min heating. Also, with increasing Pt composition, the particle diameters slightly increased and the surface of particles changed from a wavy Pt shell to a spherical dendric particle morphology (Fig. 8b). Despite the higher reduction potential of the Pt precursor than that of the Pd precursor, Pd was first reduced and formed the core, while Pt forms dendric shells on Pd nanocubes. It is considered that the Pt precursor forms a more stable complex with CTAB compared with Pd(II) ion, resulting in the slower reduction rate of the Pt precursor.[55] Therefore, Pd@Pt core-shell NPs were formed in this synthesis, even though Pt has a larger redox potential. By tuning reaction conditions and reagents, it would be possible to synthesize other core-shell or segregated alloy NPs by a single-step flow synthesis.

4. Flow Syntheses of Solid-Solution Alloy NPs

The solid-solution structure has a randomly mixed atomic arrangement in one crystal structure phase. Therefore, a concurrent chemical reduction of different metal ions is required in a continuous-flow synthesis. In this section, reaction systems and strategies for solid-solution alloy NPs are introduced.

4. 1. Single-step flow syntheses under ambient pressure

The thermodynamically stable solid-solution alloy NPs consisting of some metals that have larger redox potentials can be obtained relatively easier by a continuous-flow synthesis as well as a batch synthesis. For example, Au and Pd can form solid-solution alloys over the whole composition range,[56] and their ions are quickly reduced by strong reducing agents such as

Fig. 8 (a) Schematic of single-step continuous-flow reactor for Pd@Pt core-shell NPs. TEM images of Pd@Pt NPs synthesized at the ratio of Pd:Pt = (b) 6:1, (c) 3:1 and (d) 1:1. Scale bars are 50 nm, and the scale bars in the inset images are 10 nm. Reproduced with permission from ref. 54 Copyright 2019, American Chemical Society.


Fig. 9 (a) DF-STEM image of $Ag_{30}Rh_{70}$ NPs. Scale bar in (a) is 50 nm. The corresponding EDS maps of (b) Ag + Rh and (C) Rh and (E) Ag. Reproduced with permission from ref. 61 Copyright 2019, American Chemical Society..

NaBH$_4$ even at room temperature and ambient pressure. Therefore, many types of batch syntheses of AuPd solid-solution alloy NPs have been reported.[57–60] Cattaneo et al. also succeeded in synthesizing AuPd solid-solution NPs by a continuous-flow reactor through rapid reduction of metal ions with NaBH$_4$.[40] They used a similar setup as shown in Fig. 4a without a 4-way connection and injection of Pd solution. HAuCl$_4$ and PdCl$_2$ were mixed in H$_2$O and pumped into the reactor. Then, both metal ions were simultaneously reduced by NaBH$_4$ at the T-shaped connector and formed AuPd solid-solution alloy NPs. The alloy NPs synthesized by the continuous-flow reactor had a more homogeneous Au/Pd composition than the corresponding batch synthesis.

Malmstadt, Brutchey and Humphrey et al. used a microwave-assisted continuous-flow synthesis technique for RhAg alloy NPs.[61] Although Ag and Rh are immiscible metals in bulk, their solid-solution alloy NPs were recently synthesized by a batch synthesis[62] and a microwave-assisted synthesis.[63] The flow synthesis was performed based on the batch syntheses. A mixture of AgNO$_3$ and RhCl$_3$·xH$_2$O in a PVP ethylene glycol solution at a molar ratio of 3:7 was prepared and injected into a microwave cavity as microdroplets separated by inert Fluorinert FC-40. The droplets were heated at 120 °C for 9 min in the microwave cavity, and the synthesized NPs were separated from the solution by ultracentrifugation. STEM-EDS maps revealed that both Ag and Rh atoms coexisted in one NP (Fig. 9), indicating the AgRh solid-solution alloy NPs were obtained by a continuous-flow synthesis.

As another example, Zhang et al. used a three-layer structured microchip with an array of four parallel channels to increase the production rate of PtFeCu carbon-supported NPs (Fig. 10).[64] The metal precursor solution was prepared by adding H$_2$PtCl$_6$·6H$_2$O into a mixture of FeCl$_3$·6H$_2$O, CuCl$_2$·2H$_2$O and carbon black spheres solutions. The other solution was an H$_3$N·BH$_3$ solution (reducing agent). The metal and reducing agent solutions were injected into the front and back sides of the microchip that has symmetric dendric bifurcation, respectively. The reducing agent solution flowed to the front side through the holes at the bottom of the inlet zone and mixed with the metal precursors. The S-shaped reaction path enhances mixing by generating
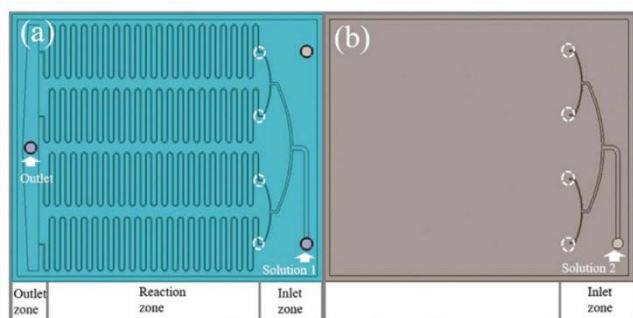
Fig. 10 Schematic of the microchip channel design. (a) The front side and (b) the backside of the microchip. White circles indicate the mixing points of the two injected solutions in the microchip. Reproduced with permission from ref. 64 Copyright 2020, Royal Society of Chemistry.

chaotic convection, resulting in the homogeneity of the product. The obtained NPs were evenly loaded on the carbon support with a narrow size distribution (for example, 1.8 $\pm$ 0.3 nm in polyethylene glycol (PEG) solution). X-ray photoelectron spectroscopy (XPS), STEM-EDS and XRD indicated the formation of a solid-solution alloy phase of the three elements, even though Fe atoms were partly segregated to the particle surface of the synthesized NPs. The alloy NPs synthesized by using PEG exhibited higher catalytic activity and stability for electrochemical methanol oxidation than the commercial Pt/C catalyst.

4. 2. Single-step flow syntheses under high pressure

To concurrently reduce different metal ions for the formation of solid-solution alloy NPs, an extreme reaction environment such as supercritical fluid has been studied instead of using strong reducing agents under ambient conditions. Since Adschiri et al. developed a synthesis method of metal oxide NPs,[65] many kinds of materials including oxides and monometallic NPs have been synthesized in supercritical fluids.[60,66–70] It is said that the reaction rate in supercritical fluids is enhanced more than 10^3 times higher than conventional hydrothermal synthesis.[71] However, the continuous-flow synthesis of alloy NPs in supercritical fluids has not been well studied. As far as we know, the first example of solid-solution alloy NPs synthesized in a continuous supercritical fluid is PtRu reported by Iversen et al. in 2017.[72] They used absolute ethanol as a solvent (reducing agent) at 200 bar and 450 °C. A mixture of Pt(acac)$_2$ (acac = acetylacetonate) and Ru(acac)$_3$ in an ethanol-toluene solution was mixed with the supercritical ethanol and passed through a reactor heated at 450 °C. STEM-EDS analysis revealed that both Ru and Pt were evenly distributed in all NPs and formed solid-solution alloy NPs. In addition, the detailed XRD analysis showed a deviation from the bulk phase diagram, that is, both face-centred cubic (fcc) and hexagonal close-packed (hcp) phases were observed in Pt$_{1-x}$Ru$_x$ (x < 0.2).

Kallesøe et al. used supercritical flow synthesis for the one-step production of PtPd and PtPdFe NPs supported on γ-Al$_2$O$_3$.[73] The alloy NPs were synthesized by simultaneous reduction of FeCl$_3$·6H$_2$O, H$_2$PtCl$_6$·6H$_2$O and PdCl$_2$ on γ-Al$_2$O$_3$ with supercritical ethanol. Fig. 11(a) shows a schematic of the flow reactor consisting of two pumps (a, b), heated reactor blocks (c, d), a pressure relief valve (e), manometers (f), solvent temperature control (g), reactor temperature control (h), a cooling system (i), precursors solution (j), solvent (k), and mixing point (m). The synthesized (PtPd)$_1$Fe$_{0.3}$/ γ-Al$_2$O$_3$ catalyst exhibited much higher catalytic activity for C$_3$H$_6$ oxidation compared with the corresponding catalyst synthesized by the conventional incipient wetness impregnation method. The crystal structure of fresh and aged (750 °C for 3 h in 10% O$_2$, 10% H$_2$O) samples was characterized by synchrotron XRD with the pair distribution function (PDF) method.[74] As shown in Fig. 11b, all of the major features were well described by a simple fcc model. Fig. 11c shows the lattice parameters extracted from

the refined models of PDF. The lattice parameter of the fresh catalysts decreases with the Fe molar ratio without any feature
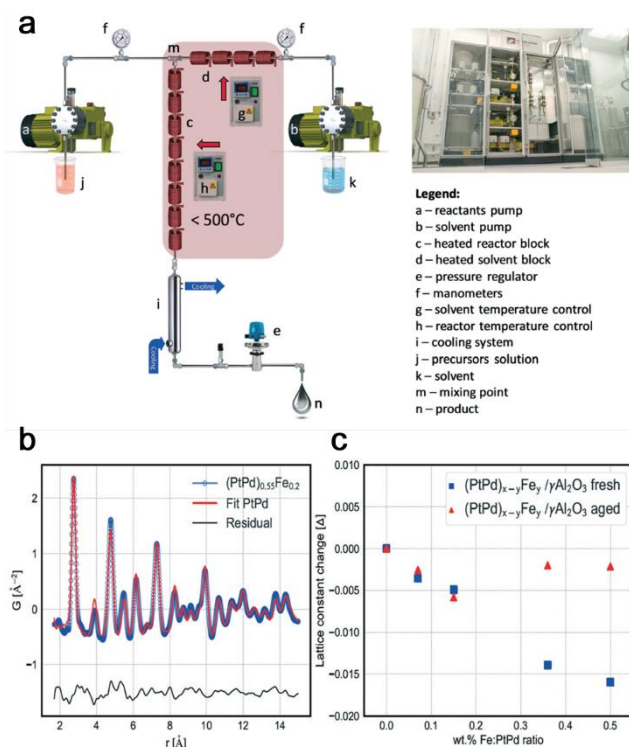
Fig. 11 (a) Schematic of a continuous-flow reactor for supercritical fluid synthesis of alloy NPs. The nucleation of NPs will be initiated at the mixing point, m, and the particle growth will be promoted in the heated reaction column, c. (b) The fitting result of PDF with a spherically attenuated fcc model (R_w = 17%). (c) The change in the lattice parameters from the background-subtracted data for PtPd and PtPdFe NPs with Fe molar ratio in the alloys. Reproduced with permission from ref. 73 Copyright 2019, Royal Society of Chemistry.

of oxide phases. This indicates the alloying of Fe with PdPt because the atomic radius of Fe is smaller than those of Pd and Pt.[75] The supercritical fluid synthesis can produce PtPdFe alloy NPs, even though Fe is hardly reduced by ethanol under ambient conditions. Recently, Kusada et al. reported successful continuous-flow syntheses of several solid-solution alloy NPs from immiscible binary to multi-element alloy NPs.[76] In addition, novel solid-solution alloy NPs consisting of immiscible elements in the bulk have been developed and have drawn huge interest because of their attractive properties that cannot be found in their parent metals.[77–81] For instance, Ru and Pd are immiscible in bulk,[82] but their solid-solution NPs were synthesized by a chemical reduction method[83] and exhibited very high catalytic activity toward nitrogen oxide (NOx) reduction in a three-way catalytic (TWC) reaction.[84] Furthermore, it was reported that the catalytic stability of PdRu was drastically enhanced by alloying with Ir because of increased configurational entropy, and the performance of PdRuIr for TWC was comparable to Rh.[85] These alloys were synthesized by a continuous-flow reactor, as shown in Fig. 12(a). The system is similar to Fig. 11(a), but this system has no additional heating after the mix point and

the chiller is located just after the mixer for rapid cooling to synthesize smaller alloy NPs with non-equilibrium solid-solution
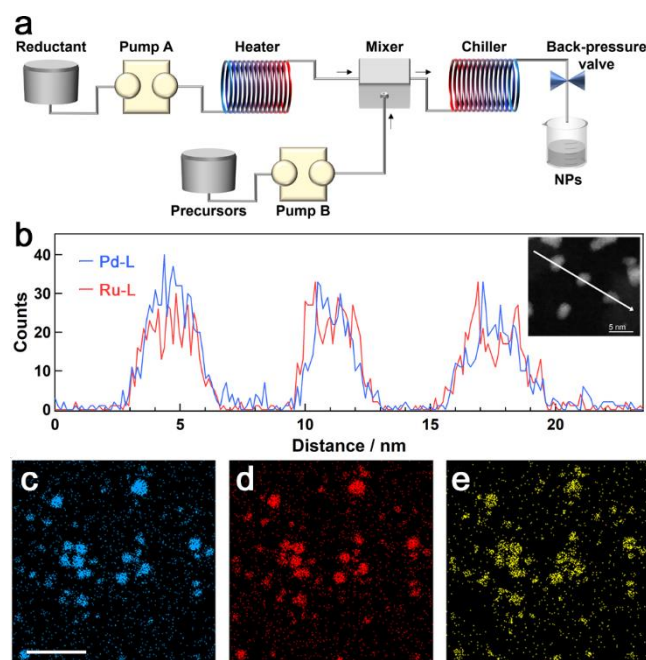

Fig. 12 (a) Schematic of a continuous-flow reactor for the synthesis of PdRu and PdRuIr NPs. (b) Pd-L and Ru-L EDS line profiles of PdRu NPs. The profiles were recorded along the white arrow in the HAADF-STEM image (inset). (c) Pd-L, (d) Ru-L and (e) Ir-M EDS maps of PdRuIr NPs. Scale bar is 20 nm. Reproduced with permission from ref. 76 Copyright 2021, American Chemical Society.

phases. K_2PdCl_4, $RuCl_3 \cdot nH_2O$ and $IrCl_4 \cdot nH_2O$ were used as the metal precursors. An aqueous solution consisting of PVP and the metal precursors at the desired molar ratio was injected into a 50 vol% ethanol aqueous solution at 230 °C, 7.0 MPa, and 250 °C, 7.0 MPa for PdRu and PdRuIr, respectively. For the synthesis of PdRuIr NPs, NaOH was added into the ethanol solution to accelerate the reduction of metal precursors. Because of rapid cooling after the reaction, the synthesized PdRu and PdRuIr NPs have smaller sizes (about 3 nm) and distributions compared with the alloy NPs synthesized by batch syntheses. XRD and STEM-EDS analyses revealed the solid-solution structures (Fig. 12(b)-(e)). PdRuIr showed very similar high catalytic activity for TWC reaction to PdRuIr catalyst obtained by the batch synthesis. These results suggested that this continuous-flow synthesis would be a suitable way for novel solid-solution alloy NPs instead of batch syntheses.

A continuous-flow synthesis is suitable for mass production because a flow-reaction system provides highly efficient productivity with high reproducibility because of stable reaction conditions. Although all the aforementioned reactor systems were studied at a laboratory scale, a pilot-scale continuous-flow reactor for alloy NPs synthesis was developed.[76] The reactor system is similar to the laboratory-scale system shown in Fig. 12(a) but was equipped with a slurry pump to allow synthesizing alloy NPs on catalyst supports such as metal oxides without

protecting agents (Fig. 13(a)). This reactor can realize extreme conditions until 30 MPa and 450 °C. Fig. 13(b) and (c) show a
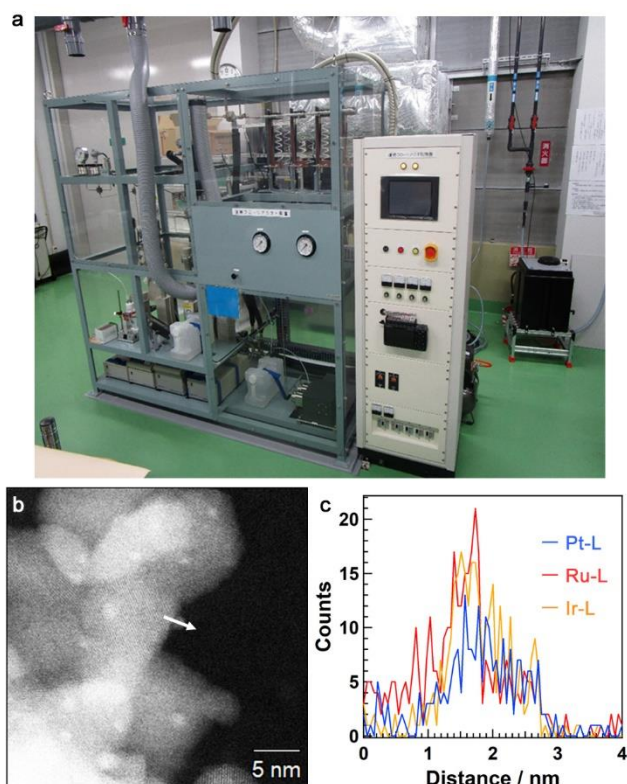

Fig. 13 (a) The pilot-scale continuous-flow reactor. (b) HAADF-STEM image of PtRuIr-CZ synthesized by (a). (c) STEM-EDS line profiles obtained along the white arrow in (b) (yellow, Ir-L; red, Ru-L; and blue, Pt-L). Reproduced with permission from ref. 76 Copyright 2021, American Chemical Society.

HAADF-STEM image and EDS line profiles of PtRuIr supported on CeO_2-ZrO_2 (CZ) synthesized by the pilot-scale reactor. The three elements exist in one particle with a diameter of ~1 nm. This reactor can produce ca. 13 kg of the catalyst containing those small alloy NPs per month. The reproducibility of this pilot-scale reactor was confirmed by the synthesis of PdRuIr-CZ for 5 h. The composition and size of the alloy NPs were not significantly changed for 5 h, indicating the high reproducibility and stability for mass production of alloy NPs.

5. Flow Syntheses of High-Entropy Alloy NPs

HEAs are solid-solution alloys composed of at least five elements with near-equimolar ratios (5–35 at%). HEAs are well studied as structural bulk materials because it has attractive mechanical properties because of a large configurational entropy.[86] Very recently, nanosized HEAs have attracted huge attention because of their high thermal and chemical stabilities and unique catalytic properties.[87–91] Therefore, the mass production of HEA NPs will be significantly desired in the near term. Although HEA NPs have been synthesized by several kinds of techniques, such as the carbon-thermal-shock method[92] and laser ablation[93], the first example of a continuous-flow synthesis of HEA NPs was done by Kusada et al.[76] This synthesis was

performed by the flow reactor shown in Fig. 12(a). IrPdPtRhRu HEA NPs were synthesized by injecting a mixed precursor
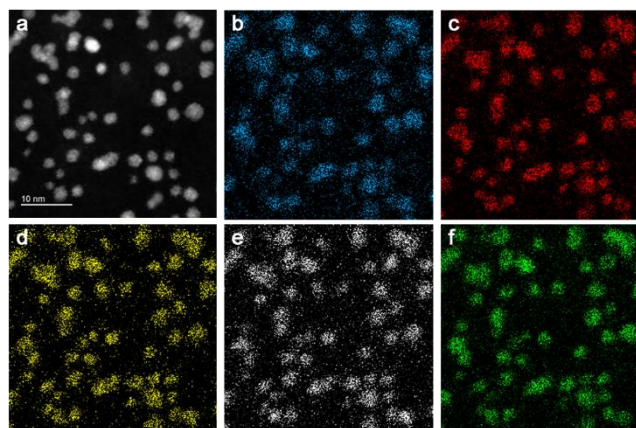
Fig. 14 (a) HAADF-STEM image of PGM-HEA NPs. The corresponding EDS maps of (b) Pd, (c) Ru, (d) Ir, (e) Pt and (f) Rh. Reproduced with permission from ref. 76 Copyright 2021, American Chemical Society.

aqueous solution of $RuCl_3 \cdot nH_2O$, $RhCl_3 \cdot 3H_2O$, $K_2[PdCl_4]$, $IrCl_4 \cdot nH_2O$, $K_2[PtCl_4]$ and PVP into 50 vol % ethanol aqueous solution with NaOH at 300 °C under a back-pressure of 9.5 MPa. The synthesized HEA NPs had a single fcc phase, and the mean diameter was 3.1 ± 0.3 nm. This is more homogeneous and smaller than IrPdPtRhRu NPs obtained by a batch synthesis.[87] STEM-EDS analysis revealed that all five elements were homogeneously distributed in each NP (Fig. 14).

6. Conclusions

In this review, we overviewed the trend in the flow syntheses of NPs. The studies on continuous-flow syntheses of NPs were found from the 2000s and continue increasing each year. Although most of the studies were on the syntheses of oxide and metallic NPs, the syntheses of alloy NPs were not well developed in the early stage because of the structural complexity compared with oxide and monometallic NPs. However, by transferring the technologies developed in the oxide and monometallic studies and generating original ideas, recently, the number of studies on the flow syntheses of alloy NPs has gradually increased. These studies proposed a variety of flow reactor systems to precisely control alloy structure in NPs. For the syntheses of segregated alloy structures, including core-shell type, multi-step type reactors are used to sequentially reduce different metal ions. On the other hand, single-step reactors are favourable to synthesize solid-solution alloy NPs through concurrent reduction of metal ions. Although the synthesized alloy NPs mainly consist of noble metals that are easily reduced by alcohol and handy reducing agents, new types of alloy NPs such as HEA and novel solid-solution alloys consisting of immiscible elements in bulk have been synthesized. Furthermore, not only laboratory-scale reactors but also a pilot-scale reactor have been successfully developed, and mass production of alloy NP catalysts has commenced.

ARTICLE   **Journal Name**

As shown in this review, outstanding progress in the continuous-flow synthesis of alloy NPs has been made over the past 10 years, and it appears that there are still some challenges and difficulties to be a universal synthesis method in industrial production. First, the elements used in flow syntheses are currently restricted compared with batch syntheses because the techniques of flow synthesis to realize special reaction environments such as inert conditions have not been well developed. Therefore, some elements easily oxidized in air and/or water have not been widely studied yet. Second, narrow flow pass clogging sometimes occurs during a reaction, because synthesizing alloy NPs generate solids in a flow. This is a serious problem that needs to be solved so realize stable and safe industrial production. The clogging causes contamination and inhomogeneous reaction conditions. To avoid clogging, the design of the flow path would be very important. The ideal flow path would be designed by taking advantage of a height difference. In addition, the choice of reagents depends on the type of pumps in the system. Although supercritical fluids are often used in the solid-solution alloy NP synthesis, pumps sending a fluid under high pressure rarely send a slurry sample. A cylinder pump can send a slurry sample and a solution generating bubbles but is not useful for continuous synthesis because it can send only the solution in the cylinder at a time. Therefore, the development of pumps will support further advancements in a continuous-flow synthesis.

Most current studies are transferring technology from batch syntheses to continuous-flow syntheses and replicating the syntheses of alloy NPs that were synthesized by batch syntheses. Because a continuous-flow reactor can realize special reaction environments including high pressure/temperature, rapid cooling, and efficient mixing that are different from batch syntheses, it would be accelerated to discover new alloy NPs synthesized by only flow reactors. In addition, by using high-throughput flow synthesis, in-situ analysis such as spectroscopy, and incorporating data science, continuous-flow synthesis of alloy NPs will attract much more attention in materials science in the near future. On line analysis of the formation of alloy NPs in the flow system is one of the most serious challenges and exciting topics and would greatly accelerate the discovery of new materials and scaling up the systems. Since X-ray, IR and UV lights cannot penetrate a thick stainless tube which is used for high pressure and/or temperature flow reactors, it is very difficult to observe the formation of alloy NPs in such flow systems. However, several papers reported on line spectroscopy in the flow system with smart designs and revealed formation mechanisms of nanoparticles in flow syntheses.[94] In addition to such laboratory scale on line analyses, developing on line analysis in such flow reactor with synchrotron techniques providing ultra-fast time resolution would be an important topic. On the other hand, some studies reported modeling and simulation of the diffusion and thermal conduction of the fluid in a flow reactor.[95,96] These studies could supplement the lack of direct on line analysis experiments and further develop this research field. In addition, as a rapidly growing technique, we should focus on machine learning. By taking advantage of a flow-reactor synthesis, we could predict a suitable reaction condition and reactor design for making new materials or scaling up the system with the help of informatics before long.

Conflicts of interest

There are no conflicts to declare.

References

1   A. Heuer-Jungemann, N. Feliu, I. Bakaimi, M. Hamaly, A. Alkilany, I. Chakraborty, A. Masood, M. F. Casula, A. Kostopoulou, E. Oh, K. Susumu, M. H. Stewart, I. L. Medintz, E. Stratakis, W. J. Parak and A. G. Kanaras, *Chem. Rev.*, 2019, **119**, 4819–4880.

2   K. Zhu, Y. Ju, J. Xu, Z. Yang, S. Gao and Y. Hou, *Acc. Chem. Res.*, 2018, **51**, 404–413.

3   Q. Wang and D. Astruc, *Chem. Rev.*, 2020, **120**, 1438–1511.

4   K. Loza, M. Heggen and M. Epple, *Adv. Funct. Mater.*, , DOI:10.1002/adfm.201909260.

5   K. Kusada, D. Wu and H. Kitagawa, *Chem. - A Eur. J.*, 2020, **26**, 5105–5130.

6   A. M. El-Toni, M. A. Habila, J. P. Labis, Z. A. Alothman, M. Alhoshan, A. A. Elzatahry and F. Zhang, *Nanoscale*, 2016, **8**, 2510–2531.

7   H. Kobayashi, K. Kusada and H. Kitagawa, *Acc. Chem. Res.*, 2015, **48**, 1551–1559.

8   K. Kusada and H. Kitagawa, *Adv. Mater.*, 2016, **28**, 1129–1142.

9   K. Geyer, J. D. C. Codée and P. H. Seeberger, *Chem. - A Eur. J.*, 2006, **12**, 8434–8442.

10   C. Wiles and P. Watts, *Green Chem.*, 2012, **14**, 38–54.

11   R. L. Hartman, J. P. McMullen and K. F. Jensen, *Angew. Chemie - Int. Ed.*, 2011, **50**, 7502–7519.

12   T. Tsubogo, H. Oyamada and S. Kobayashi, *Nature*, 2015, **520**, 329–332.

13   J. A. Darr, J. Zhang, N. M. Makwana and X. Weng, *Chem. Rev.*, 2017, **117**, 11125–11238.

14   M. Solsona, J. C. Vollenbroek, C. B. M. Tregouet, A. E. Nieuwelink, W. Olthuis, A. Van Den Berg, B. M. Weckhuysen and M. Odijk, *Lab Chip*, 2019, **19**, 3575–3601.

15   Y. Xu, V. Musumeci and C. Aymonier, *React. Chem. Eng.*, 2019, **4**, 2030–2054.

16   L. Zhang and Y. Xia, *Adv. Mater.*, 2014, **26**, 2600–2606.

17   J. Ma, S. M. Y. Lee, C. Yi and C. W. Li, *Lab Chip*, 2017, **17**, 209–226.

18   S. Duraiswamy and S. A. Khan, *Small*, 2009, **5**, 2828–2834.

19   A. A. Chaudhry, J. Goodall, M. Vickers, J. K. Cockcroft, I. Rehman, J. C. Knowles and J. A. Darr, *J. Mater. Chem.*, 2008, **18**, 5900–5908.

20   P. Boldrin, A. K. Hebb, A. A. Chaudhry, L. Otley, B. Thiebaut, P. Bishop and J. A. Darr, *Ind. Eng. Chem. Res.*, 2007, **46**, 4830–4838.

21   J. Boleininger, A. Kurz, V. Reuss and C. Sönnichsen, *Phys. Chem. Chem. Phys.*, 2006, **8**, 3824–3827.

22   Y. T. Didenko and K. S. Suslick, *J. Am. Chem. Soc.*, 2005, **127**, 12196–12197.

23   A. Yoko, G. Seong, T. Tomai and T. Adschiri, 2020, **37**, 28–41.

24   M. P. Tsang, G. Philippot, C. Aymonier and G. Sonnemann, *ACS Sustain. Chem. Eng.*, 2018, **6**, 5142–5151.

25   M. Jiao, J. Zeng, L. Jing, C. Liu and M. Gao, *Chem. Mater.*, 2015, **27**, 1299–1305.

26   R. I. Gruar, C. J. Tighe and J. A. Darr, *Ind. Eng. Chem. Res.*, 2013, **52**, 5270–5281.

27   V. Sebastian Cabeza, S. Kuhn, A. A. Kulkarni and K. F. Jensen, *Langmuir*, 2012, **28**, 7007–7013.

28   S. E. Lohse, J. R. Eller, S. T. Sivapalan, M. R. Plews and C. J. Murphy, *ACS Nano*, 2013, **7**, 4135–4150.

29   H. Mehenni, L. Sinatra, R. Mahfouz, K. Katsiev and O. M. Bakr, *RSC Adv.*, 2013, **3**, 22397–22403.

30   A. Ross, M. Muñoz, B. H. Rotstein, E. J. Suuronen and E. I. Alarcon, *Sci. Rep.*, 2021, **11**, 5420.

31   D. Saha, E. D. Bøjesen, A. H. Mamakhel, M. Bremholm and B. B. Iversen, *ChemNanoMat*, 2017, **3**, 472–478.

32   S. Cattaneo, D. Bonincontro, T. Bere, C. J. Kiely, G. J. Hutchings, N. Dimitratos and S. Albonetti, *ChemNanoMat*, 2020, **6**, 420–426.

33   M. S. Naughton, V. Kumar, Y. Bonita, K. Deshpande and P. J. A. Kenis, *Nanoscale*, 2015, **7**, 15895–15903.

34   A. Anwar, I. U. Rehman and J. A. Darr, *J. Phys. Chem. C*, 2016, **120**, 29069–29076.

35   V. N. Le, H. T. Kwon, T. K. Vo, J. H. Kim, W. S. Kim and J. Kim, *Mater. Chem. Phys.*, , DOI:10.1016/j.matchemphys.2020.123278.

36   F. Carraro, J. D. Williams, M. Linares-Moreau, C. Parise, W. Liang, H. Amenitsch, C. Doonan, C. O. Kappe and P. Falcaro, *Angew. Chemie - Int. Ed.*, 2020, **59**, 8123–8127.

37   T. Didriksen, A. I. Spjelkavik and R. Blom, *J. Flow Chem.*, 2017, **7**, 13–17.

38   A. Knauer, A. Thete, S. Li, H. Romanus, A. Csáki, W. Fritzsche and J. M. Köhler, *Chem. Eng. J.*, 2011, **166**, 1164–1169.

39   H. Song, J. D. Tice and R. F. Ismagilov, *Angew. Chemie Int. Ed.*, 2003, **42**, 768–772.

40   S. Cattaneo, S. Althahban, S. J. Freakley, M. Sankar, T. Davies, Q. He, N. Dimitratos, C. J. Kiely and G. J. Hutchings, *Nanoscale*, 2019, **11**, 8247–8259.

41   Y. Hashiguchi, F. Watanabe, T. Honma, I. Nakamura, S. S. Poly, T. Kawaguchi, T. Tsuji, H. Murayama, M. Tokunaga and T. Fujitani, *Colloids Surfaces A Physicochem. Eng. Asp.*, 2021, **620**, 126607.

42   T. Gu, C. Zheng, F. He, Y. Zhang, S. A. Khan and T. A. Hatton, *Lab Chip*, 2018, **18**, 1330–1340.

43   T. Gu, E. W. Q. Yeap, A. Somasundar, R. Chen, T. A. Hatton and S. A. Khan, *Lab Chip*, 2016, **16**, 2694–2700.

44   A. Gupta, H. B. Eral, T. A. Hatton and P. S. Doyle, *Soft Matter*, 2016, **12**, 2826–2841.

45   J. W. Hu, Y. Zhang, J. F. Li, Z. Liu, B. Ren, S. G. Sun, Z. Q. Tian and T. Lian, *Chem. Phys. Lett.*, 2005, **408**, 354–359.

46   B. Ashley, D. D. Lovingood, Y. C. Chiu, H. Gao, J. Owens and G. F. Strouse, *Phys. Chem. Chem. Phys.*, 2015, **17**, 27317–27327.

47   M. K. Bayazit, J. Yue, E. Cao, A. Gavriilidis and J. Tang, *ACS Sustain. Chem. Eng.*, 2016, **4**, 6435–6442.

48   E. B. Hostetler, K. J. Kim, R. P. Oleksak, R. C. Fitzmorris, D. A. Peterson, P. Chandran, C. H. Chang, B. K. Paul, D. M. Schut and G. S. Herman, *Mater. Lett.*, 2014, **128**, 54–59.

49   M. Nishioka, M. Miyakawa, H. Kataoka, H. Koda, K. Sato and T. M. Suzuki, *Nanoscale*, 2011, **3**, 2621–2626.

50   A. V. Nikam, A. A. Kulkarni and B. L. V. Prasad, *Cryst. Growth Des.*, 2017, **17**, 5163–5169.

51   A. M. Shanmugharaj and S. H. Ryu, *Electrochim. Acta*, 2012, **74**, 207–214.

52   J. Zhang, L. Wan, L. Liu, Y. Deng, C. Zhong and W. Hu, *Nanoscale*, 2016, **8**, 3962–3972.

53   J. H. Seog, D. Kim, Y. Kim, N. S. Kim, S. B. Lee and S. W. Han, *CrystEngComm*, 2016, **18**, 6029–6034.

54   A. Pekkari, Z. Say, A. Susarrey-Arce, C. Langhammer, H. Härelind, V. Sebastian and K. Moth-Poulsen, *ACS Appl. Mater. Interfaces*, 2019, **11**, 36196–36204.

55   Y. Kim, Y. W. Lee, M. Kim and S. W. Han, *Chem. - A Eur. J.*, 2014, **20**, 7901–7905.

56   H. Okamoto and T. B. Massalski, *Bull. Alloy Phase Diagrams*, 1985, **6**, 229–235.

57   Ö. Metin, X. Sun and S. Sun, *Nanoscale*, 2013, **5**, 910–912.

58   A. R. Wilson, K. Sun, M. Chi, R. M. White, J. M. Lebeau, H. H. Lamb and B. J. Wiley, *J. Phys. Chem. C*, 2013, **117**, 17557–17566.

59   M. Sankar, Q. He, M. Morad, J. Pritchard, S. J. Freakley, J. K. Edwards, S. H. Taylor, D. J. Morgan, A. F. Carley, D. W. Knight, C. J. Kiely and G. J. Hutchings, *ACS Nano*, 2012, **6**, 6600–6613.

60   Ž. Knez, E. Markočič, M. Leitgeb, M. Primožič, M. Knez Hrnčič and M. Škerget, *Energy*, 2014, **77**, 235–243.

61   P. Kunal, E. J. Roberts, C. T. Riche, K. Jarvis, N. Malmstadt, R. L. Brutchey and S. M. Humphrey, *Chem. Mater.*, 2017, **29**, 4341–4350.

62   K. Kusada, M. Yamauchi, H. Kobayashi, H. Kitagawa and Y. Kubota, *J. Am. Chem. Soc.*, 2010, **132**, 15896–15898.

63   S. García, L. Zhang, G. W. Piburn, G. Henkelman and S. M. Humphrey, *ACS Nano*, 2014, **8**, 11512–11521.

64   Y. Zhou, D. Wang, X. Kang, D. Zhang, X. Dou, X. Wang and G. Guo, *Nanoscale*, 2020, **12**, 12647–12654.

65   T. Adschiri, K. Kanazawa and K. Arai, *J. Am. Ceram. Soc.*, 1992, **75**, 1019–1022.

66   Y. Kimura, D. Abe, T. Ohmori, M. Mizutani and M. Harada, *Colloids Surfaces A Physicochem. Eng. Asp.*, 2003, **231**, 131–141.

67   C. Aymonier, A. Loppinet-Serani, H. Reverón, Y. Garrabos and F. Cansell, *J. Supercrit. Fluids*, 2006, **38**, 242–251.

68   T. Adschiri, Y. W. Lee, M. Goto and S. Takami, *Green Chem.*, 2011, **13**, 1380–1390.

69   D. Sanli, S. E. Bozbag and C. Erkey, *J. Mater. Sci.*, 2012, **47**, 2995–3025.

70   X. Zhang, S. Heinonen and E. Levänen, *RSC Adv.*, 2014, **4**, 61137–61152.

71   H. Hayashi and Y. Hakuta, *Materials (Basel).*, 2010, **3**, 3794–3817.

72   M. Bondesgaard, A. Mamakhel, J. Becker, H. Kasai, G. Philippot, M. Bremholm and B. B. Iversen, *Chem. Mater.*, 2017, **29**, 3265–3273.

73   H. Silva, P. Hernandez-Fernandez, A. K. Baden, H. L. Hellstern, A. Kovyakh, E. Wisaeus, T. Smitshuysen, I. Chorkendorff, L. H. Christensen, D. Chakraborty and C. Kallesøe, *Catal. Sci. Technol.*, 2019, **9**, 6691–6699.

74   P. J. Chupas, X. Qiu, J. C. Hanson, P. L. Lee, C. P. Grey and S. J. L. Billinge, *J. Appl. Crystallogr.*, 2003, **36**, 1342–1347.

75   R. Abazari, F. Heshmatpour and S. Balalaie, *ACS Catal.*, 2013, **3**, 139–149.

76   K. Kusada, T. Yamamoto, T. Toriyama, S. Matsumura, K. Sato, K. Nagaoka, K. Terada, Y. Ikeda, Y. Hirai and H. Kitagawa, *J. Phys. Chem. C*, 2021, **125**, 458–463.

77   K. Kusada, D. Wu, T. Yamamoto, T. Toriyama, S. Matsumura, W. Xie, M. Koyama, S. Kawaguchi, Y. Kubota and H. Kitagawa, *Chem. Sci.*, 2019, **10**, 652–656.

78   K. Mori, K. Miyawaki and H. Yamashita, *ACS Catal.*, 2016, **6**, 3128–3135.

79   Q. Zhang, K. Kusada, D. Wu, N. Ogiwara, T. Yamamoto, T. Toriyama, S. Matsumura, S. Kawaguchi, Y. Kubota, T. Honma and H. Kitagawa, *Chem. Sci.*, 2019, **10**, 5133–5137.

80   F. Wang, K. Kusada, D. Wu, T. Yamamoto, T. Toriyama, S. Matsumura, Y. Nanba, M. Koyama and H. Kitagawa, *Angew. Chemie - Int. Ed.*, 2018, **0395**, 4505–4509.

81   K. Kusada, M. Yamauchi, H. Kobayashi, H. Kitagawa and Y. Kubota, *J. Am. Chem. Soc.*, 2010, **132**, 15896–15898.

82   D. Wu, K. Kusada and H. Kitagawa, *Sci. Technol. Adv. Mater.*, 2016, 1–14.

83   K. Kusada, H. Kobayashi, R. Ikeda, Y. Kubota, M. Takata, S. Toh, T. Yamamoto, S. Matsumura, N. Sumi, K. Sato, K. Nagaoka and H. Kitagawa, *J. Am. Chem. Soc.*, 2014, **136**, 1864–1871.

84   K. Sato, H. Tomonaga, T. Yamamoto, S. Matsumura, N. D. B. Zulkifli, T. Ishimoto, M. Koyama, K. Kusada, H. Kobayashi, H. Kitagawa and K. Nagaoka, *Sci. Rep.*, 2016, **6**, 28265.

85   K. Kusada, D. Wu, Y. Nanba, M. Koyama, T. Yamamoto, X. Q. Tran, T. Toriyama, S. Matsumura, A. Ito, K. Sato, K. Nagaoka, O. Seo, C. Song, Y. Chen, N. Palina, L. S. R. Kumara, S. Hiroi, O. Sakata, S. Kawaguchi, Y. Kubota and H. Kitagawa, *Adv. Mater.*, 2021, **33**, 1–7.

86   M. H. Tsai and J. W. Yeh, *Mater. Res. Lett.*, 2014, **2**, 107–123.

87   D. Wu, K. Kusada, T. Yamamoto, T. Toriyama, S. Matsumura, I. Gueye, O. Seo, J. Kim, S. Hiroi, O. Sakata, S. Kawaguchi, Y. Kubota and H. Kitagawa, *Chem. Sci.*, 2020, **11**, 12731–12736.

88   Y. Yao, Z. Liu, P. Xie, Z. Huang, T. Li, D. Morris, Z. Finfrock, J. Zhou, M. Jiao, J. Gao, Y. Mao, J. Miao, P. Zhang, R. Shahbazian-Yassar, C. Wang, G. Wang and L. Hu, *Sci. Adv.*, 2020, **6**, 1–12.

89   P. Xie, Y. Yao, Z. Huang, Z. Liu, J. Zhang, T. Li, G. Wang, R. Shahbazian-Yassar, L. Hu and C. Wang, *Nat. Commun.*, 2019, **10**, 1–12.

90   T. Löffler, A. Savan, H. Meyer, M. Meischein, V. Strotkötter, A. Ludwig and W. Schuhmann, *Angew. Chemie - Int. Ed.*, 2020, **59**, 5844–5850.

91   D. Wu, K. Kusada, T. Yamamoto, T. Toriyama, S. Matsumura, S. Kawaguchi, Y. Kubota and H. Kitagawa, *J. Am. Chem. Soc.*, 2020, **142**, 13833–13838.

92   L. Hu, P. Xie, R. Shahbazian-Yassar, Y. Yao, S. D. Lacey, J. Li, R. J. Jacob, C. Wang, H. Xie, A. Nie, Z. Huang, F. Chen, M. Rehwoldt, D. Yu, M. R. Zachariah and T. Pu, *Science (80-.).*, 2018, **359**, 1489–1494.

93   F. Waag, Y. Li, A. R. Ziefuß, E. Bertin, M. Kamp, V. Duppel, G. Marzun, L. Kienle, S. Barcikowski and B. Gökce, *RSC Adv.*, 2019, **9**, 18547–18558.

94   I. Lignos, Y. Mo, L. Carayannopoulos, M. Ginterseder, M. G. Bawendi and K. F. Jensen, *React. Chem. Eng.*, 2021, **6**, 459–464.

95   C. Y. Ma, X. Z. Wang, C. J. Tighe and J. A. Darr, *IFAC Proc. Vol.*, 2012, **8**, 874–879.

96   C. Y. Ma, J. J. Liu, Y. Zhang and X. Z. Wang, *J. Supercrit. Fluids*, 2015, **98**, 211–221.